Letter

Weak dissipation for high-fidelity qubit-state preparation and measurement

Anthony Ransford,[1,*,†] Conrad Roman,[1,2,3,*] Thomas Dellaert,[1,2,3] Patrick McMillin,[1,2,3] and Wesley C. Campbell[1,2,3]

[1]*Department of Physics & Astronomy, University of California Los Angeles, Los Angeles, California, USA*
[2]*Challenge Institute for Quantum Computation, University of California Los Angeles, Los Angeles, California, USA*
[3]*Center for Quantum Science and Engineering, University of California Los Angeles, Los Angeles, California, USA*

(Received 2 September 2021; accepted 14 December 2021; published 29 December 2021)

We demonstrate a method of qubit state preparation and measurement (SPAM) based on a weakly open quantum channel that achieves a higher fidelity than previous demonstrations, even with low detection efficiency. The trapped-ion qubit SPAM infidelity ($2.1^{+0.5}_{-0.4} \times 10^{-4}$) is limited by setup-specific errors from ion loss and imperfect population transfer between qubit eigenstates, and we show that full transfer would yield an inaccuracy less than 8×10^{-5}. The high precision of this method revealed errors caused by a rare ($\approx 10^{-4}$ likelihood) magnetic-dipole decay that we measure and correct by driving an additional transition. Since this scheme allows fluorescence collection for effectively unlimited periods, high fidelity is achievable even with limited optical access and low quantum efficiency photon detectors.

DOI: 10.1103/PhysRevA.104.L060402

Recent progress in quantum device fidelity has focused primarily on improving unitary operations, i.e., single- and multiqubit gates, with some small systems achieving gate infidelities below thresholds necessary for fault tolerant encodings [1–3]. Despite these improvements, current systems lack the capacity to encode a computationally useful number of fault tolerant logical qubits. As such, current devices fall in the noisy intermediate scale quantum (NISQ) category [4], where operations are performed without fault tolerance and the state preparation and measurement (SPAM) fidelity of an N qubit register will typically decrease exponentially with size as $(\mathcal{F}_{\mathrm{SPAM}})^N$ where $\mathcal{F}_{\mathrm{SPAM}}$ is the single-qubit fidelity.

Using strong dissipation [$\gamma/2\pi = O(\mathrm{MHz})$] to "shelve" an electron to a metastable state [5], the state preparation and measurement of a single qubit has recently been demonstrated with an infidelity $1 - \mathcal{F}_{\mathrm{SPAM}} = 2.9(3) \times 10^{-4} = -35.4(5)$ dB [6]. (Here and below, we express small errors ϵ in decibels as $10\log_{10}(\epsilon)$, which reduces the amount of exponential and asymmetric uncertainty notation required). The ultimate fidelity of this technique is limited by off-resonant coupling to nearby strong electric dipole ($E1$) transition error channels during the shelving process and the finite lifetimes of the metastable states. As an alternative to using strong transitions for population transfer, weak dissipative channels can also be used as a pathway to metastable states with a high degree of certainty [7,8]. Since nearby error channels are also likely to be correspondingly weak, this can afford both highly selective transfer and high quality readout of the final qubit state [7].

In this Letter, we demonstrate and characterize the use of a weak dissipative channel in $^{171}\mathrm{Yb}^+$ hyperfine qubits to perform qubit state preparation and measurement with inaccuracy approaching 10^{-4}. An electric-quadrupole ($E2$) transition is driven by a laser to irreversibly transfer population from one qubit state to the effectively stable $^2F^o_{7/2}$ state in $O(100\ \mathrm{ms})$ [7,9,10]. The long lifetime of this state (≈ 2 years [11]) allows for laser-induced fluorescence to be collected for essentially unlimited duration without metastable decay, and we are able to distinguish the ground state from the metastable manifold with an inaccuracy <-52 dB (single-sided 90% confidence interval) without high efficiency imaging. The increased precision allotted by this technique revealed a qubit mixing error caused by a rare magnetic-dipole ($M1$) decay ($A_{M1} = 2\pi \times 4.1^{+2.3}_{-1.5}$ mHz) during population transfer, which we demonstrate can be corrected by introducing another laser beam. We achieve a ground-state hyperfine qubit SPAM inaccuracy $\epsilon_{\mathrm{SPAM}} = -39(1)$ dB, limited by the fidelity of unitary population transfer required to prepare one of the qubit states. While narrowband optical pumping requires a longer duration [here, $O(100\ \mathrm{ms})$] than a typical gate $O(100\ \mu\mathrm{s})$, it is on par with the total algorithm times in current quantum systems [12] and is appropriate for initialization and readout of NISQ devices for which faulty SPAM will require the algorithm to be rerun.

The weak dissipation scheme we present here requires a transition that is both narrow (for high state selectivity) and leaky (for robust, irreversible transfer). The $E2$ transition in Yb^+ at 411 nm connecting the ground $^2S_{1/2}$ state to $^2D_{5/2}$ has a $\gamma = 2\pi \times 22$ Hz linewidth, decays primarily to the $^2F^o_{7/2}$ state, and has been investigated as a potential frequency standard [13,14] and as a probe for physics beyond the standard model [15]. The extremely long lifetime of the $^2F^o_{7/2}$ state and its optical isolation from the $^{171}\mathrm{Yb}^+$ cooling cycle at 369 nm makes it an ideal location to store qubit population during laser-induced fluorescence for state detection, and we use the 411 nm transition as the weakly open channel to this state, as shown in Fig. 1.

Selection rules allow for a quasicycling $E2$ transition on $^2S_{1/2}(F=1) \leftrightarrow {}^2D_{5/2}(F=3)$ to state-selectively optically pump one $^{171}\mathrm{Yb}^+$ hyperfine level to $^2F^o_{7/2}$ with

*These authors contributed equally to this work.
†ransfordanthony@gmail.com

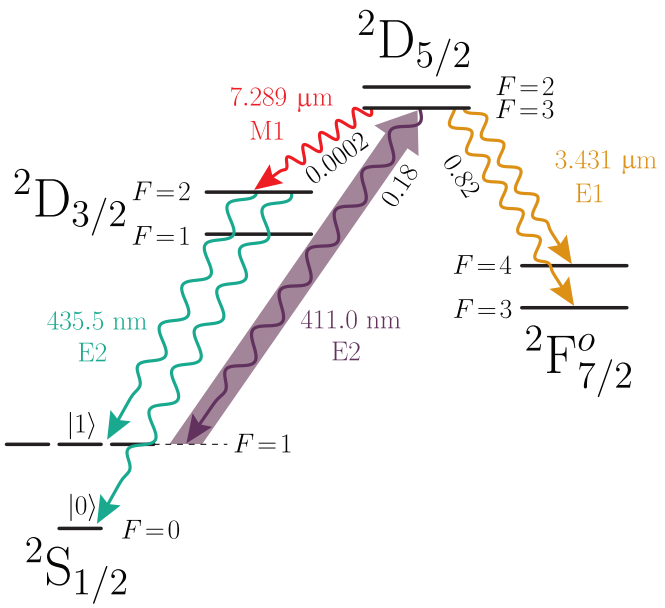

FIG. 1. Electron shelving of the $|1\rangle$ state via weak dissipation for high fidelity readout. The $M1$ fine-structure decay shown can induce a SPAM error due to its potential eventual decay to $|0\rangle$. Each transition is labeled with its leading order identification as an electric-dipole ($E1$), electric-quadrupole ($E2$), or magnetic-dipole ($M1$) process.

$E2$-decay-induced mixing. The large hyperfine splitting of the intermediate $^2D_{5/2}$ state (191 MHz [14]) relative to $\gamma/2\pi$ minimizes the likelihood of off-resonant scattering, and the stability of the metastable state makes state misidentification due to spontaneous emission of the now hidden population a nonissue. Following narrowband population transfer, subsequent laser interrogation reveals any population remaining in the $^2S_{1/2}$ state with a high degree of certainty.

The ground-state qubit is defined on the zero-field hyperfine clock states in $^{171}Yb^+$, $|^2S_{1/2}; F=0, M_F=0\rangle \equiv |0\rangle$ and $|^2S_{1/2}; F=1, M_F=0\rangle \equiv |1\rangle$, with operating frequency $\omega_q = 2\pi \times 12.64$ GHz. The ion is trapped in an oblate Paul trap driven at $\Omega_{RF} = 2\pi \times 49$ MHz with typical secular frequencies of $(\omega_x, \omega_y, \omega_z) \approx 2\pi \times (540, 550, 1170)$ kHz [16]. Light emitted by the ion in the $+z$ direction is focused by an off-the-shelf objective through an iris directly onto a PMT yielding a modest overall photon detection efficiency of ≈0.16%. A magnetic field of 4.4 G is applied in the $+z$ direction to lift the degeneracy of magnetically sensitive states. All lasers propagate in the xy plane, perpendicular to the applied magnetic field. Qubit rotations are performed by microwave radiation delivered by an *ex vacuo* standard gain horn antenna.

To evaluate the effectiveness of weak dissipative transfer of the $|1\rangle$ state to $^2F^o_{7/2}$ for qubit measurement, we determine the accuracy of state preparation and electron shelving measurement of a single qubit by repeating SPAM attempts for each qubit basis state. Each experiment begins by Doppler cooling a single ion, after which laser light resonant with the $^2S_{1/2}(F=1) \leftrightarrow {}^2P^o_{1/2}(F=1)$ transition is applied for 750 μs to prepare the $|0\rangle$ state [17] with high fidelity (estimated error < -57 dB). For SPAM of the $|1\rangle$ state, after preparation of $|0\rangle$, resonant microwaves are used to transfer population to $|1\rangle$. This transition frequency is calibrated periodically by performing Ramsey spectroscopy, and we find that the relative qubit-oscillator frequency drift is typically less than 20 Hz over 24 hours. The microwave interrogation times are calibrated every 2000 experiments.

Once state preparation is complete, 2 mW of 411 nm laser light is directed onto the ion with a spot size of ≈40 μm $1/e^2$ intensity diameter in order to transfer population in the $|1\rangle$ state to the $^2F^o_{7/2}$ states through the $^2D_{5/2}(F=3)$ manifold. Applying this light, a Rabi rate of $\Omega \approx 2\pi \times 200$ kHz is inferred from the AC Stark shift of the microwave-frequency qubit. Light at 935 nm is also applied to repump any population in the $^2D_{3/2}$ state [18]. The 411 and 935 nm light is applied for 200 ms, long enough to theoretically ensure a population transfer infidelity of < -50 dB out of $^2S_{1/2}(F=1)$. The polarization of the 411 nm light is chosen to maximize the transition strengths of the $|\Delta M_F| = 2$ transitions ($\mathbf{k} \perp \hat{\boldsymbol{\epsilon}} \perp \mathbf{B}$). We transfer using the $\Delta M_F = -2$ transition due to its larger detuning from $^2D_{5/2}(F=2)$. Since the g factors of the $^2S_{1/2}(F=1)$ and $^2D_{5/2}(F=3)$ manifolds are nearly equal ($\Delta g_F \approx 10^{-3}$), all magnetic sublevels in $^2S_{1/2}(F=1)$ are coupled to $^2D_{5/2}(F=3)$ with a single laser frequency.

After electron shelving, we detect any remaining $^2S_{1/2}$ population by laser-induced fluorescence for 17 ms. Any fluorescence photons collected from the ion are counted by a custom FPGA-based pulse sequencer [19]. Population that has been shelved to the $^2F^o_{7/2}$ manifold does not produce laser-induced fluorescence.

Following state detection, population in $^2F^o_{7/2}$ is "deshelved" by driving the $E2$ transition to $^1[3/2]^o_{3/2}$ at 760 nm for 35 ms. Due to the hyperfine structure in the $^2F^o_{7/2}$ and the excited $^1[3/2]^o_{3/2}$ states, two 760 nm tones separated by 5.257 GHz are applied for quick depopulation [20]. To ensure efficient return to the ground state during deshelving, lasers at 976 and 935 nm are used to depopulate the $^2D_{5/2}$ and $^2D_{3/2}$ states via $^1[3/2]^o_{3/2}$ and $^3[3/2]^o_{1/2}$, respectively. Population is returned to the ground state manifold with a $1/e$ time of 350 μs. During deshelving, the lasers used for Doppler cooling are also applied.

While gathering data, we monitor the number of photons counted during Doppler cooling and use a threshold to restart experiments where an ion was not properly cooled *prior to* a state preparation and measurement attempt. Experiments where only the Doppler cooling counts *following* the SPAM attempt fall below the threshold are flagged as ion-loss events. We reserve the use of the term "infidelity" to include errors from ion-loss events, because those are errors that can only be identified after the fact. However, since ion loss events are flagged by low subsequent Doppler cooling counts, they can be identified and screened out to ensure they do not result in a misidentification of the qubit state, and we use the term "inaccuracy" to refer to SPAM errors not flagged as ion-loss events.

To experimentally measure the SPAM inaccuracy, we adhered to a blinded data analysis to avoid introducing bias when choosing the thresholds for Doppler cooling and state discrimination. Prior to the measurement of the final data set, ≈10^4 experiments per qubit state were performed, and appropriate thresholds for state discrimination and Doppler cooling were set and fixed based on those calibration data. The final data

TABLE I. Error budget for SPAM measurement determined from theoretical estimates and auxiliary measurements. $|0\rangle$ state preparation errors are common to both the $|0\rangle$ state and the $|1\rangle$ state, while the other sources of error apply only to either the $|1\rangle$ or the $|0\rangle$ state.

	Predicted error ($\times 10^{-4}$)	
Error source	$\|1\rangle$ state	$\|0\rangle$ state
$\|0\rangle$ state preparation	<0.02	<0.02
Unflagged error from ion loss		$0.1^{+0.2}_{-0.06}$
$\|0\rangle \rightarrow \|1\rangle$ transfer	0.74(10)	
Finite shelving time	0.06(3)	
$M1$ decay	0.82(3)	
Predicted average inaccuracy	$0.9^{+0.2}_{-0.1}$ ($-40.5^{+0.9}_{-0.1}$ dB)	
Error flagged by ion loss		$2.9^{+0.6}_{-0.5}$
Predicted average infidelity	$2.4^{+0.4}_{-0.3}$ ($-36.2^{+0.7}_{-0.6}$ dB)	

set was then unblinded and analyzed using those thresholds, resulting in 5×10^4 data points per state after removing errors flagged as ion loss events.

Following this procedure, we observe a total state preparation and measurement inaccuracy $\epsilon_{\mathrm{SPAM}} = -39(1)$ dB, where the uncertainty is a one sigma Wilson score interval. (The SPAM infidelity, which counts errors from ion loss events as failures, is $1 - \mathcal{F}_{\mathrm{SPAM}} = -36.8^{+1.0}_{-0.9}$ dB.) These results are consistent with the prediction of the error budget shown in Table I. The photon count histograms are shown in Fig. 2 and show clear separation of the two distributions, illustrating that the SPAM accuracy is not limited by the ability to distinguish the $^2S_{1/2}$ manifold from the $^2F^o_{7/2}$ manifold. Figure 3 shows high contrast qubit Rabi flopping detected using this method.

The sources of SPAM inaccuracy are asymmetric between the two qubit states. The SPAM inaccuracy of the $|0\rangle$ state

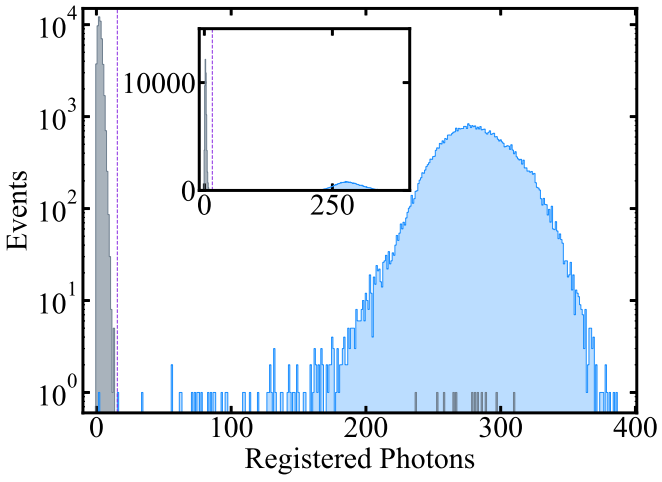

FIG. 2. Fluorescence detection count histograms for attempted SPAM of the $|1\rangle$ (blue, lighter) and $|0\rangle$ (gray, darker) ground-state hyperfine qubit states in $^{171}\mathrm{Yb}^+$. The inset shows the same data on a linear scale. The predetermined state detection threshold is shown as a dashed purple line and gives an average SPAM inaccuracy of $-39(1)$ dB.

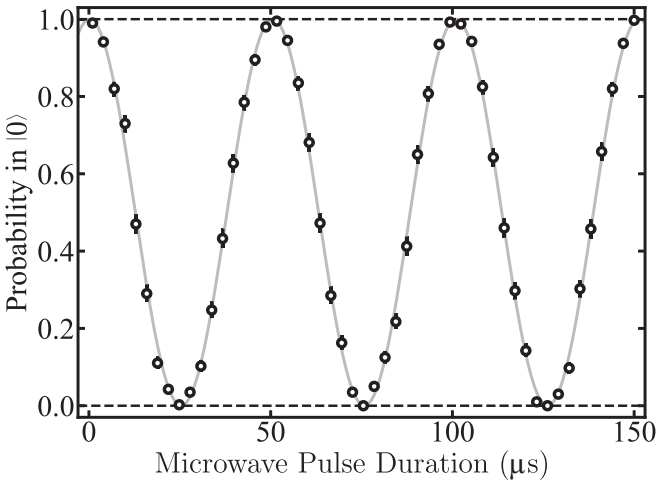

FIG. 3. High contrast readout of microwave rotations of a $^{171}\mathrm{Yb}^+$ ground-state hyperfine qubit measured via electron shelving with ≈400 measurements per point.

is found be $-47(4)$ dB, roughly $10\times$ lower than that of the $|1\rangle$ state, $-36(1)$ dB. The asymmetry comes from two sources: imperfect microwave transfer on $|0\rangle \rightarrow |1\rangle$ causing preparation of the $|1\rangle$ state to fail, and spontaneous $M1$ decay during shelving from $^2D_{5/2}(F = 3)$ to $^2D_{3/2}(F = 2)$ that subsequently decays to $|0\rangle$, causing shelving to fail (both are described below).

We quantified the quality of our microwave rotations by performing single-qubit-gate randomized benchmarking [21], finding that the infidelity of our randomized single computational gates is $\epsilon_\pi = -41.3(6)$ dB [18]. In the final data set, by subtracting the amount of shelving error we expect to be contributed from the $M1$ decay and the finite shelving time, we find that the remaining error is $-39(2)$ dB, which we therefore attribute to this imperfect transfer.

With higher fidelity state preparation of the $|1\rangle$ state, the state detection error from the fine structure $M1$ transition becomes the dominant source of SPAM inaccuracy for transfer times longer than 150 ms. The $^2S_{1/2}(F = 1)$ manifold can be prepared with higher probability than just its $|M_F = 0\rangle$ quantum state by performing a series of three, successive π rotations from $|0\rangle$ to the three $^2S_{1/2}(F = 1)$ magnetic sublevels. Figure 4 shows the measured probability of finding an unshelved ion, if it is first prepared in this way, as a function of the shelving illumination time. The green circles show the measured error with the 935 nm repump light on during shelving (which only partially protects against decay to $|0\rangle$ during the shelving of a $|1\rangle$ ion). The shelving error with this scheme is given approximately by

$$\epsilon_{\mathrm{s}}(t) = \frac{\tau_{\mathrm{D}} A_{M1}}{3\zeta} + \left(1 - \frac{\zeta}{2}\right) \exp\left(-\frac{t\zeta}{2\tau_{\mathrm{D}}}\right), \qquad (1)$$

which assumes $\tau_{\mathrm{D}} A_{M1} \ll 1$ and that all of the ^2D_J population has decayed before fluorescence querying. Here, $\zeta = 0.824(4)$ is the branching ratio to the $^2F^o_{7/2}$ manifold [22], and $\tau_{\mathrm{D}} = 7.2(3)$ ms is the lifetime of the $^2D_{5/2}$ state [13]. Using a theoretically estimated value for $A_{M1} = 2\pi \times 4.5$ mHz [18]

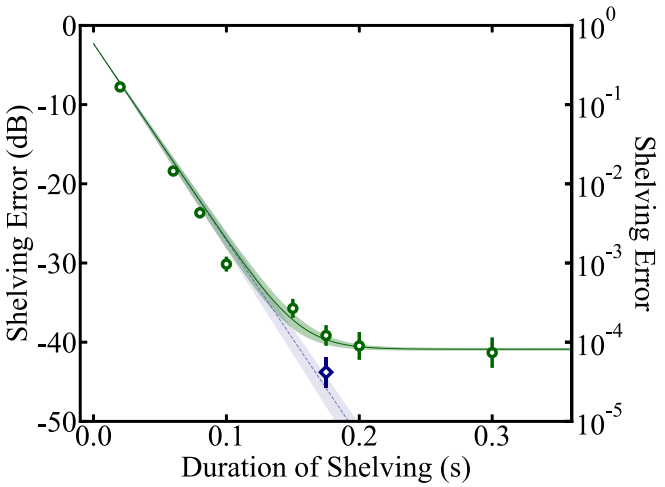

FIG. 4. Error in electron shelving of an ion prepared initially in the $^2S_{1/2}(F = 1)$ manifold as a function of 411 nm illumination times. The green, solid curve and circles show the error with only the 935 nm light repumping population from the $^2D_{3/2}$ states, while the blue, dashed curve and diamond show the error with the 935 nm light replaced by the 861 nm repump scheme. Dashed lines are the theoretical prediction of Eq. (1), with bands indicating the uncertainty in the model due to uncertainty in the $^2D_{5/2}$ lifetime and $E1$-$E2$ branching ratio. The prediction with the 861 nm repump (blue) is just the second term in Eq. (1).

yields a predicted error contribution of $\epsilon_{M1} = \epsilon_s(t \to \infty) = -40.8(2)$ dB, where the uncertainty comes from the uncertainty in τ_D. The presence of this underappreciated decay channel highlights the importance of measuring and including the shelving error when reporting state detection errors, because it is not possible to achieve qubit state detection error lower than ≈ -40 dB with this scheme without somehow addressing this source of infidelity.

The magnetic transition dipole moment between the ^2D_J levels can be measured by counting shelving errors caused by this decay using the same procedure, and the infidelity can be traced entirely to the $M1$ decay pathway at a shelving time of 300 ms. This measured error yields an $M1$ transition rate of $A_{M1} = 2\pi \times 4.1^{+2.3}_{-1.5}$ mHz, consistent with the theoretical estimate [18]. The measured decay rate corresponds to a branching ratio of $1.8^{+1.0}_{-0.7} \times 10^{-4}$ for the $^2D_{5/2} \to {}^2D_{3/2}$ decay channel.

This error channel does not set a fundamental limit to this method because it can be further suppressed with the addition of light that repumps this population via a higher angular-momentum state. Laser light at 861 nm or 1.35 μm can be used to state-selectively depopulate the $^2D_{3/2}(F = 2)$ level through $^1[3/2]^o_{3/2}(F = 2)$ or $^2P^o_{3/2}(F = 2)$, respectively, both of which decay via $E1$ transitions quickly and predominantly to the $^2S_{1/2}(F = 1)$ manifold. The blue diamond in Fig. 4 shows the measured effect on hyperfine manifold shelving of adding an 861 nm laser (and removing the 935 nm light) to mitigate the $M1$ decay error for a shelving time of 175 ms. We find that the measured shelving error is reduced by about 4 dB by this repump scheme. A binomial test applied to these two data points confirms this as a statistically significant suppression of the error mode ($p = 0.0038$).

We also measure how well we can distinguish ions in the $^2S_{1/2}$ manifold from ions in the $^2F^o_{7/2}$ manifold. This is by far the most straightforward part of this technique and should not be confused with qubit SPAM fidelity, which must include all of the error sources described above. We perform this measurement by laser cooling and counting photons produced by two ions that are either both prepared in the $^2S_{1/2}$ manifold or with precisely one excited to the $^2F^o_{7/2}$ manifold. Photons are counted in 10 ms bins, with every even bin taken as a detection bin, and the complementary odd bins taken as a check for a properly cooled ion crystal before and after a detection bin to check for and eliminate storage errors from the data set. We find that we can distinguish an ion in the metastable manifold from an ion in the ground state with a single-sided, 95% confidence interval inaccuracy limit $\epsilon_{SvsF} < -52$ dB.

One of the attractive features of the 411 nm electron shelving qubit readout scheme in $^{171}Yb^+$ [7] is the practically unlimited number of fluorescence photons that bright-manifold ions can emit. This can aid statistical rejection of fluorescence cross-talk due to the overlap of an imaging system's point spread functions from neighboring ions in a Coulomb crystal. However, care must be taken to ensure that the single $\lambda = 3.4$ μm photon that must be spontaneously emitted by each ion being shelved does not deshelve neighboring ions, as the resonant absorption cross section $[O(\lambda^2)]$ spans a length scale that may be similar to the interion spacing. In this case, it should be possible to utilize the AC Stark shift from continuous 411 nm illumination to make each ion's 3.4 μm resonance frequency unique, avoiding superradiant and reabsorption effects. Experimental studies of these effects are needed to assess their impact on large-scale systems.

Improving the speed with which qubit population can be state-selectively transferred to $^2F^o_{7/2}$ and reducing the laser intensity required to return $^2F^o_{7/2}$ state population to the laser cooling cycle are two important areas in which this scheme can be improved. To improve shelving speed, qubit population can be coherently transferred to the metastable state instead of relying on the relatively slow $E1$ decay at 3.4 μm. This can be done either directly at 467 nm [23], or using both 411 nm and 3.4 μm light, as was recently demonstrated [10]. Likewise, high speed, low intensity depopulation of the $^2F^o_{7/2}$ state should be achievable with 3.4 μm and 976 nm light.

The authors acknowledge Justin Christensen, David Hucul, Nils Huntemann, and Eric Hudson for helpful discussions. This work was partially supported by the U.S. Army Research Office under Grant No. W911NF-15-1-0261 and the U.S. National Science Foundation under Awards No. PHY-1912555 and No. OMA-2016245.

[1] E. Knill, R. Laflamme, and W. Zurek, arXiv:quant-ph/9610011 v3.

[2] A. Y. Kitaev, *Quantum Communication, Computation, and Measurement* (Springer, Boston, MA, 1997), pp. 181–188.

[3] D. Aharonov and M. Ben-Or, SIAM J. Comput. **38**, 1207 (2008).

[4] J. Preskill, Quantum **2**, 79 (2018).

[5] H. G. Dehmelt, Bull. Am. Phys. Soc. **20**, 60 (1975).

[6] J. E. Christensen, D. Hucul, W. C. Campbell, and E. R. Hudson, npj Quantum Inf. **6**, 35 (2020).
[7] C. Roman, A. Ransford, M. Ip, and W. C. Campbell, New J. Phys. **22**, 073038 (2020).
[8] D. Hayes, D. Stack, B. Bjork, A. C. Potter, C. H. Baldwin, and R. P. Stutz, Phys. Rev. Lett. **124**, 170501 (2020).
[9] C. L. Edmunds, T. R. Tan, A. R. Milne, A. Singh, M. J. Biercuk, and C. Hempel, Phys. Rev. A **104**, 012606 (2021).
[10] H. X. Yang, J. Y. Ma, Y. K. Wu, Y. Wang, M. M. Cao, W. X. Guo, Y. Y. Huang, L. Feng, Z. C. Zhou, and L. M. Duan, arXiv2106.14906.
[11] R. Lange, A. A. Peshkov, N. Huntemann, C. Tamm, A. Surzhykov, and E. Peik, Phys. Rev. Lett. **127**, 213001 (2021).
[12] J. M. Pino, J. M. Dreiling, C. Figgatt, J. P. Gaebler, S. A. Moses, M. S. Allman, C. H. Baldwin, M. Foss-Feig, D. Hayes, K. Mayer, C. Ryan-Anderson, and B. Neyenhuis, Nature (London) **592**, 209 (2021).
[13] P. Taylor, M. Roberts, S. V. Gateva-Kostova, R. B. M. Clarke, G. P. Barwood, W. R. C. Rowley, and P. Gill, Phys. Rev. A **56**, 2699 (1997).
[14] M. Roberts, P. Taylor, S. V. Gateva-Kostova, R. B. M. Clarke, W. R. C. Rowley, and P. Gill, Phys. Rev. A **60**, 2867 (1999).
[15] I. Counts, J. Hur, D. P. L. Aude Craik, H. Jeon, C. Leung, J. C. Berengut, A. Geddes, A. Kawasaki, W. Jhe, and V. Vuletić, Phys. Rev. Lett. **125**, 123002 (2020).
[16] B. Yoshimura, M. Stork, D. Dadic, W. C. Campbell, and J. K. Freericks, EPJ Quantum Technol. **2**, 2 (2015).
[17] S. Olmschenk, K. C. Younge, D. L. Moehring, D. N. Matsukevich, P. Maunz, and C. Monroe, Phys. Rev. A **76**, 052314 (2007).
[18] See Supplemental Material at http://link.aps.org/supplemental/10.1103/PhysRevA.104.L060402 for more comprehensive atomic level diagram and details of the $M1$ estimate and data analysis.
[19] T. Pruttivarasin and H. Katori, Rev. Sci. Instrum. **86**, 115106 (2015).
[20] S. Mulholland, H. A. Klein, G. P. Barwood, S. Donnellan, P. B. R. Nisbet-Jones, G. Huang, G. Walsh, P. E. G. Baird, and P. Gill, Rev. Sci. Instrum. **90**, 033105 (2019).
[21] E. Knill, D. Leibfried, R. Reichle, J. Britton, R. B. Blakestad, J. D. Jost, C. Langer, R. Ozeri, S. Seidelin, and D. J. Wineland, Phys. Rev. A **77**, 012307 (2008).
[22] T. R. Tan, C. L. Edmunds, A. R. Milne, M. J. Biercuk, and C. Hempel, Phys. Rev. A **104**, L010802 (2021).
[23] R. Lange, N. Huntemann, J. M. Rahm, C. Sanner, H. Shao, B. Lipphardt, C. Tamm, S. Weyers, and E. Peik, Phys. Rev. Lett. **126**, 011102 (2021).